RSCPublishing Faraday Discussions

Classical and nonclassical effects in surface hopping methodology for simulating coupled electronic-nuclear dynamics

SCHOLARONE™
Manuscripts

Journal Name

Classical and nonclassical effects in surface hopping methodology for simulating coupled electronic-nuclear dynamics

Craig C. Martens[*][a]

In this paper, we analyze the detailed quantum-classical behavior of two alternative approaches to simulating molecular dynamics with electronic transitions: the popular fewest switches surface hopping (FSSH) method, introduced by Tully in 1990 [Tully, *J. Chem. Phys.*, 1990, **93**, 1061] and our recently developed quantum trajectory surface hopping (QTSH) method [Martens, *J. Phys. Chem. A*, 2019 **123**, 1110]. Both approaches employ an independent ensemble of trajectories that undergo stochastic transitions between electronic surfaces. The methods differ in their treatment of energy conservation, with FSSH imposing conservation of the classical kinetic plus potential energy by rescaling the classical momentum when a surface hop occurs while QTSH incorporates a quantum force throughout the dynamics which leads naturally to the conservation of the full quantum-classical energy. We investigate the population transfer and energy budget of the surface hopping methods for several simple model systems and compare with exact quantum results. In addition, the detailed dynamics of the trajectory ensembles in phase space are compared with the quantum evolution in the Wigner representation. Conclusions are drawn.

1 Introduction

Trajectory surface hopping is a simple and efficient method for simulating the coupled electronic and nuclear dynamics of molecular systems in a quantum-classical framework[1–11]. The most popular approach is the fewest switches surface hopping (FSSH) method, originally introduced by Tully in 1990[1]. Since that original work, many researchers have employed and extended the approach in a range of physical contexts (see, e.g.,[9–11] for reviews). In FSSH, the dynamics of the fully quantum nuclear wavepacket evolving on coupled electronic surfaces is approximated by an ensemble of classical trajectories, each of which evolves independently. This classical motion is combined with stochastic transitions, or "hops" between the coupled electronic states. To determine the hopping probabilities, a proxy electronic Schrödinger equation that evolves under the influence of the time dependent classical variables is carried by each trajectory. Fewest switches surface hopping has proven to be a simple and robust method for the simulation of molecular dynamics with electronic transitions.

Despite its utility and popularity, there are a number of issues with FSSH that inspire continuing work on developing surface

hopping methodology. The FSSH approach is based on using an ensemble of independent trajectories. This is an approximation to the fundamental nonlocality and indivisibility of quantum *states*, and leads to some inaccuracies. One problem is that the independent trajectories do not represent quantum coherence—and especially decoherence—properly, leading to a representation of the quantum evolution that is *overcoherent*, in the sense that the off-diagonal quantum density matrix elements of individual trajectories can be spuriously large in magnitude compared to the exact quantum coherence. Attempts to improve FSSH have focused mainly on corrections to this problem; a number of approaches to incorporating decoherence corrections to FSSH are reviewed in Ref.[10]. Another characteristic of FSSH is strict classical energy conservation imposed on the individual trajectories when they undergo transitions between electronic states. In particular, when a hop occurs, the corresponding difference in electronic state energies at the transition point is accommodated in the nuclear dynamics by an *ad hoc* rescaling of the momentum along the nonadiabatic coupling vector. This algorithm is—quite reasonably—based on recognizing the importance of classical energy conservation, but has no rigorous foundation based on first principles. The FSSH algorithm also results in practical problems, such as the spurious closing of classically-forbidden channels allowed by the full quantum evolution and the presence of so-called

[a] *Department of Chemistry, University of California, Irvine, Irvine, CA 92697-2025, USA. Fax: +1-949-824-8571; Tel: +1-949-824-8768; E-mail: cmartens@uci.edu*

"frustrated hops"—transitions that are dictated to occur by the surface hopping stochastic process but rejected by the imposition of classical energy conservation. These events degrade the consistency of surface hopping, defined as the agreement between the evolving quantum density matrix probabilities and the state populations reflected by the statistics of the hopping trajectory ensemble. Further, the reliance of the FSSH algorithm on using the nonadiabatic coupling vector in the momentum rescaling leads to a theory that is only well-defined in the adiabatic representation of electronic states, losing the important property of representation independence and limiting FSSH to modeling multidimensional systems in the adiabatic representation.

Recently, we proposed an alternative surface hopping framework, *Consensus Surface Hopping* (CSH),[12,13] which was developed with the goal of rigorously incorporating the nonclassical effects of nonlocality, uncertainty, and quantum coherence[14] in a surface hopping context. The method is based on a quantum-classical limit of the multi-state quantum Liouville equation[15–21] in the framework of a trajectory ensemble representation of the full density matrix in the Wigner representation. The advantages of CSH come at a cost, however, and the interdependence of the trajectories in the ensemble makes the method numerically much more expensive than FSSH.

The greatest value of the CSH formalism, in our opinion, is not as a numerical method *per se* but as a framework for developing additional approximations and more economical methodology in a well-controlled and rigorous manner.

We recently derived an approximate independent trajectory limit of CSH, which we call *Quantum Trajectory Surface Hopping* (QTSH)[13]. In the independent trajectory limit, we obtain a statistical surface hopping algorithm that is equivalent to the standard FSSH stochastic trajectory hopping result. The main difference with FSSH is the abandonment of the physically-motivated but *ad hoc* momentum rescaling to impose classical energy conservation at the individual trajectory level and its replacement by *quantum forces* derived rigorously from the semiclassical-limit quantum-classical Liouville equation. QTSH restores the consistency of surface hopping that is broken by the frustrated hops of the standard FSSH approach. Unlike FSSH, the QTSH algorithm maintains the time reversibility of the evolving state *on average*: individual trajectories are not time reversible due to their stochastic nature, but the densities that they collectively represent evolve in a time-reversible manner. In addition, the energetics of the system are treated correctly: the full quantum-classical energy is conserved rigorously at the ensemble level. The ensemble average energy conservation is the correct behavior required by quantum mechanics; individual trajectory conservation of the classical energy is a constraint that is too restrictive and *too classical*, and so precludes important quantum effects. A detailed report on the QTSH formalism can be found in Ref.[13].

In this paper, we present a comparison of the behavior of the QTSH and FSSH methodologies for several very simple systems. We examine the time dependent population transfer dynamics of the surface hopping methods and compare the results with exact quantum wavepacket calculations. The energy budget of the QTSH method is also analyzed. In addition, we visualize snapshots of the trajectory ensembles in phase space and compare with Wigner functions calculated from the wavepacket results. General conclusions are drawn from the observed behavior.

2 Theory

We begin by briefly reviewing the the key elements of the FSSH and QTSH approaches. More detailed discussions can be found in the papers cited.

2.1 Fewest Switches Surface Hopping (FSSH)

The Fewest Switches Surface Hopping (FSSH) method was proposed by John Tully in 1990[1]. The FSSH formalism starts with the Hamiltonian describing the electronic and nuclear degrees of a molecular system, given by

$$\hat{H} = \hat{T}_{\mathbf{q}} + \hat{H}_o(\mathbf{r}, \mathbf{q}). \tag{1}$$

Here, $\mathbf{r}$ and $\mathbf{q}$ are the electronic and nuclear coordinates, respectively. $\hat{T}_{\mathbf{q}}$ is the nuclear kinetic energy operator while $\hat{H}_o(\mathbf{r}, \mathbf{q})$ is the electronic Hamiltonian, which depends parametrically on the nuclear coordinates $\mathbf{q}$. An electronic basis is chosen, $\phi_n(\mathbf{r}; \mathbf{q})$, which are functions of the electronic coordinates $\mathbf{r}$ and may also depend parametrically on the nuclear coordinates $\mathbf{q}$. In this basis, the Hamiltonian matrix elements are

$$V_{mn}(\mathbf{q}) = \int \phi_m^*(\mathbf{r}; \mathbf{q}) \hat{H}_o(\mathbf{r}, \mathbf{q}) \phi_n(\mathbf{r}; \mathbf{q}) d\mathbf{r}. \tag{2}$$

In the adiabatic representation, the electronic wavefunctions depend on $\mathbf{q}$, and the derivative coupling matrix element $\mathbf{d}_{mn}(\mathbf{q})$ results from off-diagonal matrix elements of the nuclear kinetic energy:

$$\mathbf{d}_{mn}(\mathbf{q}) = \int \phi_m^*(\mathbf{r}; \mathbf{q}) \nabla_{\mathbf{q}} \phi_n(\mathbf{r}; \mathbf{q}) d\mathbf{r}. \tag{3}$$

The FSSH formalism uses classical trajectories and ensemble averaging to approximate the nuclear quantum dynamics of a multicomponent wavepacket. These trajectories represent the quantum electronic transitions by undergoing stochastic transitions—the "hops" of surface hopping—between the electronic surfaces. The electronic dynamics in the chosen basis are coupled to the time-dependent nuclear trajectories $\mathbf{q}(t)$ which appear in the nuclear coordinate dependence of the electronic Hamiltonian. For a given classical path $\mathbf{q}(t)$ the electronic wavefunction can be expanded as

$$\psi(\mathbf{r}, t) = \sum_n c_n(t) \phi_j(\mathbf{r}; \mathbf{q(t)}). \tag{4}$$

Substitution into the time-dependent Schrödinger equation yields a set of coupled differential equations for the expansion coefficients:

$$i\hbar \dot{c}_m(t) = \sum_n (V_{mn} - i\hbar \dot{\mathbf{q}} \cdot \mathbf{d}_{mn}) c_n(t). \tag{5}$$

In terms of the electronic density matrix $a_{mn} = c_m c_n^*$ the quantum equations of motion become

$$i\hbar \dot{a}_{mn}(t) = \sum_l \left[(V_{ml} - i\hbar \dot{\mathbf{q}} \cdot \mathbf{d}_{ml}) a_{ln} - a_{ml} (V_{ln} - i\hbar \dot{\mathbf{q}} \cdot \mathbf{d}_{ln}) \right], \tag{6}$$

where $\mathbf{d}_{ln}^* = -\mathbf{d}_{nl}$ and $\mathbf{d}_{nn} = 0$.

The equation of motion for the population of the nth state, represented by the diagonal density matrix element a_{nn}, is then given by:

$$\dot{a}_{nn} = \sum_{l \neq n} b_{nl}, \qquad (7)$$

where

$$b_{nl} = \frac{2}{\hbar} \text{Im}(a_{nl}^* V_{nl}) - 2\text{Re}(a_{nl}^* \dot{\mathbf{q}} \cdot \mathbf{d}_{nl}). \qquad (8)$$

In the FSSH method, an ensemble of trajectories $(\mathbf{q}_j(t), \mathbf{p}_j(t))$ $(j = 1, 2, \cdots, N)$ are sampled from a distribution representing the initial nuclear quantum state, where $\mathbf{p}_j$ is the canonical momentum conjugate to the jth trajectory's nuclear coordinate $\mathbf{q}_j$. Each trajectory so generated is initiated on one of the electronic states and then evolves independently and classically under Hamilton's equations that correspond to the instantaneous occupied state. Each trajectory carries its own copy of the electronic density matrix $a_{mn,j}$, which is the independent ensemble member's "proxy" for the full quantum electronic-nuclear density matrix.

Stochastic transitions occur between these states with a probability that is proportional to the relative rate of change of the quantum populations associated with the trajectory's proxy density matrix. For instance, for a two state system with the jth trajectory currently occupying surface 1, its probability of hopping from surface 1 to surface 2 during a time step of duration Δt is given by

$$P_{hop}^{FSSH}(t) = \left| \frac{1}{a_{11}(t)} b_{12}(t) \Delta t \right| \qquad (9)$$

if $\dot{a}_{11,j}$ is negative and zero otherwise.

The hop is realized or not by generating a random number between 0 and 1 and comparing it with $P_{hop}^{FSSH}(t)$. An analogous procedure is used for a trajectory currently on state 2.

Strict classical energy conservation at level of the individual trajectory is strictly imposed by rescaling the momentum at the instant of the hop. In multidimensional systems, the momentum rescaling is performed along the direction of the nonadiabatic coupling vector $\mathbf{d}_{12}$. If insufficient energy is available for an upward hop in energy, the event is termed "frustrated" and does not occur despite the stochastic algorithm dictating the transition. Such aborted events lead to a breakdown of the consistency between the density matrix populations and the trajectory ensemble statistics.

2.2 Quantum Trajectory Surface Hopping (QTSH)

The FSSH approach yields a physically well-motivated but *ad hoc* method for simulating nonadiabatic dynamics with trajectories. Recently, we introduced the Consensus Surface Hopping (CSH) formalism, which seeks to go beyond this and build a trajectory-based method for nonadiabatic dynamics simulations with a rigorous foundation [12,13]. The CSH approach focuses on solving the multistate quantum Liouville equation for coupled electronic and nuclear dynamics in the semiclassical limit using trajectory ensembles to represent phase space densities [15–19]. From this perspective, the density matrix evolves quantum mechanically, and so the trajectory dynamics must correspondingly become nonclassical. We briefly sketch the derivation of CSH and the additional approximations underlying the QTSH method under discussion in

the present paper.

CSH and QTSH are based in solving the full quantum density matrix evolution in the quantum-classical limit using stochastic trajectory ensembles. We therefore start with the quantum mechanical Liouville equation for the density operator $\hat{\rho}(t)$, given by [22]

$$i\hbar \frac{d\hat{\rho}(t)}{dt} = [\hat{H}, \hat{\rho}(t)], \qquad (10)$$

where $\hat{H}$ is the Hamiltonian of the system. For dynamics on a single potential surface, the classical limit of Eq. (10) is simply the classical Liouville equation [23],

$$\frac{\partial \rho}{\partial t} = \{H, \rho\}, \qquad (11)$$

where $\rho(\mathbf{q}, \mathbf{p}, t)$ and $H(\mathbf{q}, \mathbf{p}, t)$ are now functions of the $2f$-dimensional (for f nuclear degrees of freedom) phase space variables $\Gamma = (\mathbf{q}, \mathbf{p})$ and time t, and $\{H, \rho\}$ is the Poisson bracket of H and ρ: $\{H, \rho\} = \partial H / \partial \mathbf{q} \cdot \partial \rho / \partial \mathbf{p} - \partial \rho / \partial \mathbf{q} \cdot \partial H / \partial \mathbf{p}$. This correspondence can be derived systematically from Eq. (10) by performing a Wigner-Moyal expansion [24,25] of the quantum mechanical Liouville equation. To lowest order in $\hbar$, this involves replacing commutators by Poisson brackets: $[\hat{A}, \hat{B}] \rightarrow i\hbar\{A, B\} + O(\hbar^2)$.

The semiclassical limit of Eq. (10) can be generalized to two coupled quantum states further coupled to classical degrees of freedom. The approach is general for mixed quantum-classical problems. Here we first consider the specific case of two quantum electronic states in the diabatic electronic representation coupled to classical limit nuclear dynamics. The Hamiltonian and density matrix are given by 2×2 matrices:

$$\hat{H} = \begin{pmatrix} \hat{H}_{11} & \hat{V} \\ \hat{V} & \hat{H}_{22} \end{pmatrix} \qquad (12)$$

and

$$\hat{\rho}(t) = \begin{pmatrix} \hat{\rho}_{11}(t) & \hat{\rho}_{12}(t) \\ \hat{\rho}_{21}(t) & \hat{\rho}_{22}(t) \end{pmatrix}, \qquad (13)$$

respectively. The elements of these matrices are nuclear operators, which become classical phase space functions in the quantum-classical limit. The result are coupled classical-like Liouville equations [15–19,26–31]:

$$\frac{\partial \rho_{11}}{\partial t} = \{H_{11}, \rho_{11}\} + \{V, \alpha\} - \frac{2V}{\hbar}\beta \qquad (14)$$

$$\frac{\partial \rho_{22}}{\partial t} = \{H_{22}, \rho_{22}\} + \{V, \alpha\} + \frac{2V}{\hbar}\beta \qquad (15)$$

$$\frac{\partial \alpha}{\partial t} = \{H_0, \alpha\} + \omega\beta + \frac{1}{2}\{V, \rho_{11} + \rho_{22}\} \qquad (16)$$

$$\frac{\partial \beta}{\partial t} = \{H_0, \beta\} - \omega\alpha + \frac{V}{\hbar}(\rho_{11} - \rho_{22}). \qquad (17)$$

The coherence $\rho_{12}(\Gamma, t) = \alpha(\Gamma, t) + i\beta(\Gamma, t)$ is expressed above in terms of its real and imaginary parts, and we have defined the average Hamiltonian $H_0 = (H_{11} + H_{22})/2$ and frequency $\omega = (H_{11} - H_{22})/\hbar$. All higher order terms in $\hbar$ have been neglected, leading to a classical-limit formalism that retains only the most important nonclassical corrections.

The CSH method employs a trajectory ensemble representation

of the phase space functions describing the density matrix in the coupled semiclassical Liouville equations. Quantum population transfer is represented by stochastic trajectory hops between the diagonal surfaces while quantum coherence is represented collectively at the ensemble level by interrelationships between nonclassical amplitudes and phases associated with each trajectory. We emphasize that our trajectory ensemble is not a statistical ensemble representing a mixed state but instead a *quantum* ensemble that corresponds to a trajectory basis of the evolving *pure* state quantum dynamics.

The phase space densities corresponding to the populations of states 1 and 2 are together represented by a single ensemble of N trajectories, each of which is characterized by a point in phase space $\Gamma_j(t) = (\mathbf{q}_j(t), \mathbf{p}_j(t))$ and a binary integer $\sigma_j(t)$, which can take on the values 1 or 0, indicating whether the trajectory is associated with quantum state 1 or 2, respectively. In the numerical implementation involving finite trajetory ensembles, the δ functions are smoothed using phase space Gaussians, as described in Ref. [12]. This results in the replacement of the delta functions by the Gaussian basis $g(\Gamma)$: $\delta(\Gamma - \Gamma_j) \rightarrow g(\Gamma - \Gamma_j)$.

The coherence $\rho_{12}(\Gamma, t)$ is also represented in terms of the trajectory ensemble. Unlike the populations, however, the coherence is a complex quantity and thus the coefficients of the trajectories are complex numbers. The populations and the real and imaginary parts of the coherence are given in terms of the smoothed trajectory ensemble as:

$$\rho_{11}(\Gamma, t) = \frac{1}{N} \sum_{j=1}^{N} \sigma_j(t) g(\Gamma - \Gamma_j(t)) \qquad (18)$$

$$\rho_{22}(\Gamma, t) = \frac{1}{N} \sum_{j=1}^{N} \left(1 - \sigma_j(t)\right) g(\Gamma - \Gamma_j(t)) \qquad (19)$$

$$\alpha(\Gamma, t) = \frac{1}{N} \sum_{j=1}^{N} \alpha_j(t) g(\Gamma - \Gamma_j(t)) \qquad (20)$$

$$\beta(\Gamma, t) = \frac{1}{N} \sum_{j=1}^{N} \beta_j(t) g(\Gamma - \Gamma_j(t)). \qquad (21)$$

The coefficients $\sigma_j(t)$ are stochastic binary integers, while $\alpha_j(t)$ and $\beta_j(t)$ $(j = 1, 2, \ldots, N)$ are continuous real numbers. (See Ref. [32] for an alternative approach to the general problem of quantum state hopping that represents both populations and coherence in terms of separate stochastic processes.)

In the full CSH formalism, the equations of motion for the trajectories $\Gamma_j(t)$ and state parameters $(\sigma_j(t), \alpha_j(t), \beta_j(t))$ $(j = 1, 2, \ldots, N)$ are determined by subtituting the trajectory representations, Eqs. (18)–(21), into the semiclassical Liouville equations (14)–(17). Two types of nonclassical terms appear. The first are sink and source terms $\pm 2V\beta/\hbar$, which are responsible for the population transfer between states. The second type of nonclassical terms are the Poisson brackets $\{V, \alpha\}$, which appear symmetrically in the equations for both ρ_{11} and ρ_{22}. These interactions modify the shape of the evolving distributions, but do not change the total state populations. Conservation of population under these terms results from the fact that the classical trace (integral over phase space) of a Poisson bracket vanishes for functions

satisfying appropriate boundary conditions.

The evolution of the dynamical variables is determined by integrating numerically the ordinary differential equations for the trajectories and the coefficients. Each time step of duration Δt is divided into two parts. First, the coefficients are updated and then the phase space trajectories are propagated forward in time.

As derived in Ref. [12], the CSH stochastic hopping probability for a trajectory transition from surface 1 to surface 2 is

$$P_{hop}^{CSH} = \left| \frac{2}{\hbar \langle \rho_{11} \rangle_j} V(\Gamma_j) \langle \beta \rangle_j \Delta t \right|, \qquad (22)$$

where

$$\langle \rho_{11} \rangle_j = \frac{1}{N} \sum_{k=1}^{N} \sigma_k g(\Gamma_j - \Gamma_k) \qquad (23)$$

and

$$\langle \beta \rangle_j = \frac{1}{N} \sum_{k=1}^{N} \beta_k g(\Gamma_j - \Gamma_k) \qquad (24)$$

are the local values of the *functions* ρ_{11} and β at the phase space point Γ_j, with an analogous expression for hops from 2 to 1.

The result in Eq. (22) is strongly reminiscent of the FSSH hopping probability given in Eq. (9). But we emphasize the essential difference between this approach and the FSSH method. Here, the ensemble collectively determines the stochastic hopping probabilities of each of its members. The local densities $\langle \rho_{11} \rangle_j$ and $\langle \rho_{22} \rangle_j$ and the coherence $\langle \beta \rangle_j$ at point Γ_j depend on the *ensemble* of evolving trajectories $\Gamma_k(t)$ $(k = 1, 2, \ldots, N)$. They are not independent dynamical variables associated with independent trajectories, as in the FSSH formalism. Quantum transitions are thus determined by a "consensus" among the members of the ensemble representing the full entangled electronic-nuclear quantum state, rather than by the independent trajectories of FSSH.

The coherence parameters obey the equations

$$\dot{\alpha}_j = \omega(\Gamma_j) \beta_j \qquad (25)$$

$$\dot{\beta}_j = [-\omega(\Gamma_j) \alpha_j + \frac{1}{\hbar} V(\Gamma_j)(2\sigma_j - 1)]. \qquad (26)$$

These differential equations are integrated numerically using standard methods.

We emphasize that no artificial decoherence is added to the evolving system in the CSH formalism. The role played by coherence and its decay is treated accurately through the collective nature of the method as highlighted by Eq. (24). In particular, decoherence is represented naturally *via* cancellation of the signed terms β_k in the summation over Γ_k in the local vicinity of the hopping trajectory j to yield $\langle \beta \rangle_j$. If these terms exhibit destructive interference due to either the nature of the pure state evolution of the multicomponent nuclear wavepacket or by environmental fluctuations in the difference potential $\omega(\Gamma_k)$ over the ensemble, then this summation will be "decayed" by decoherence. The individual β_k values may be quite large; it is only the *weighted sum* of their values $\langle \beta \rangle_j$ that becomes small with decoherence. In contrast, FSSH determines hopping probabilities by using the independent individual values of each trajectory's quantum density matrix. This difference is the origin of the overcoherence problem

of FSSH.

We now consider the terms in the evolution equations that involve trace-preserving Poisson brackets. These include both the homogeneous classical phase space evolution terms of the form $\{H,\rho\}$ and the inhomogeneous nonclassical terms $\{V,\alpha\}$ coupling the density matrix elements.

We consider the total nuclear density $\rho = \rho_{11} + \rho_{22}$:

$$\rho(\mathbf{q},\mathbf{p},t) = \rho_{11}(\mathbf{q},\mathbf{p},t) + \rho_{22}(\mathbf{q},\mathbf{p},t) = \frac{1}{N}\sum_{j=1}^{N} g(\Gamma - \Gamma_j(t)). \quad (27)$$

This quantity is independent of the stochastic parameters $\sigma_j(t)$. The total nuclear density $\rho(\mathbf{q},\mathbf{p},t)$ obeys the partial differential equation obtained by adding Eqs. (14) and (15):

$$\frac{\partial \rho}{\partial t} = \{H_{11}, \rho_{11}\} + \{H_{22}, \rho_{22}\} + 2\{V, \alpha\}. \quad (28)$$

The terms $\pm 2V\beta/\hbar$ responsible for population transfer between states 1 and 2 cancel from the evolution equation. Equation (28) conserves the total population, given by the phase space trace of ρ, as it should.

The equations of motion for $\mathbf{q}_j(t)$ and $\mathbf{p}_j(t)$ ($j = 1, 2, \ldots, N$) are derived by substituting Eq. (27) into Eq. (28). As described in Refs. [12,13], we obtain modified classical equations of motion for the trajectory ensemble:

$$\dot{\mathbf{q}}_j = \frac{\mathbf{p}_j}{m} \quad (29)$$

$$\dot{\mathbf{p}}_j = -\nabla U_j(\mathbf{q}_j) - 2\alpha_j \nabla V(\mathbf{q}_j) \quad (30)$$

for $j = 1, 2, \cdots, N$, where $U_j(\mathbf{q})$ is the diabatic potential of the state currently occupied by the jth trajectory and $\nabla \equiv \partial/\partial\mathbf{q}$. In addition to the classical diabatic force acting on the jth trajectory an additional *quantum force* appears. This nonclassical force depends on both the gradient of the off-diagonal diabatic coupling $V(\mathbf{q}_j)$ and the real part of the coherence $\alpha_j(t)$ corresponding to that trajectory and contributes to the dynamics whenever coupling and coherence are present. In the present formalism, these replace the sudden impulsive momentum rescalings of FSSH. Each trajectory *does not* conserve the classical energy $H_j(t)$. Rather, the total energy expectation value $E(t) = \text{Tr}(\hat{H}\hat{\rho}(t))$ is conserved on average over the ensemble [14], as we discuss in detail below. (We have considered the energetics and other issues of general quantum trajectory methods in previous publications [33–36].)

The CSH method can be implemented equally well in the adiabatic representation, where electronic state coupling appears through off-diagonal terms in the kinetic energy [17,37,38]. The quantum mechanical Hamiltonian and density matrix in the adiabatic representation are given by

$$\hat{H} = \begin{pmatrix} \hat{H}_{++} & \hat{W} \\ \hat{W}^\dagger & \hat{H}_{--} \end{pmatrix} \quad (31)$$

and

$$\hat{\rho}(t) = \begin{pmatrix} \hat{\rho}_{++}(t) & \hat{\rho}_{+-}(t) \\ \hat{\rho}_{-+}(t) & \hat{\rho}_{--}(t) \end{pmatrix}, \quad (32)$$

respectively. The adiabatic eigenstates $\{|+\rangle, |-\rangle\}$ are defined in terms of the diabatic basis $\{|1\rangle, |2\rangle\}$ as

$$|+\rangle = |1\rangle \cos(\phi/2) + |2\rangle \sin(\phi/2) \quad (33)$$

$$|-\rangle = -|1\rangle \sin(\phi/2) + |2\rangle \cos(\phi/2), \quad (34)$$

where the mixing angle $\phi(\mathbf{q})$ is given by

$$\tan\phi(\mathbf{q}) = \frac{2V(\mathbf{q})}{U_1(\mathbf{q}) - U_2(\mathbf{q})}. \quad (35)$$

Here, $U_1(\mathbf{q})$ and $U_2(\mathbf{q})$ are the diagonal diabatic state potentials and $V(\mathbf{q})$ is the off-diagonal diabatic coupling.

In terms of these states, the off-diagonal nonadiabatic couplings are

$$\hat{W} = \langle +|\hat{T}|-\rangle = \frac{i\hbar}{2m}\nabla\phi(\mathbf{q})\cdot\hat{\mathbf{p}} + \frac{\hbar^2}{4m}\nabla^2\phi(\mathbf{q}) \quad (36)$$

and

$$\hat{W}^\dagger = \langle -|\hat{T}|+\rangle = -\hat{W}. \quad (37)$$

The nonadiabatic coupling vector matrix element $\mathbf{d}(\mathbf{q})$ is defined as

$$\mathbf{d}(\mathbf{q}) \equiv \langle +|\nabla|-\rangle = -\frac{1}{2}\nabla\phi(\mathbf{q}). \quad (38)$$

By evaluating the Wigner transform of the quantum Liouville equation in the adiabatic representation, Eq. (10), to lowest order in $\hbar$ we obtain the corresponding semiclassical Liouville equations in the adiabatic representation [12,17,37]:

$$\frac{\partial \rho_{++}}{\partial t} = \{H_{++}, \rho_{++}\} - \hbar\left\{\mathbf{d}\cdot\frac{\mathbf{p}}{m}, \beta\right\} - 2\mathbf{d}\cdot\frac{\mathbf{p}}{m}\alpha \quad (39)$$

$$\frac{\partial \rho_{--}}{\partial t} = \{H_{--}, \rho_{--}\} - \hbar\left\{\mathbf{d}\cdot\frac{\mathbf{p}}{m}, \beta\right\} + 2\mathbf{d}\cdot\frac{\mathbf{p}}{m}\alpha \quad (40)$$

$$\frac{\partial \alpha}{\partial t} = \{H_o, \alpha\} + \omega\beta + \mathbf{d}\cdot\frac{\mathbf{p}}{m}(\rho_{++} - \rho_{--}), \quad (41)$$

$$\frac{\partial \beta}{\partial t} = \{H_o, \beta\} - \omega\alpha - \frac{\hbar}{2}\left\{\mathbf{d}\cdot\frac{\mathbf{p}}{m}, \rho_{++} + \rho_{--}\right\}, \quad (42)$$

where $H_{++}(\Gamma) = \mathbf{p}^2/2m + E_+(\mathbf{q})$, $H_{--}(\Gamma) = \mathbf{p}^2/2m + E_-(\mathbf{q})$, $H_o = \frac{1}{2}(H_{++} + H_{--})$, and $\omega(\Gamma) = (E_+(\mathbf{q}) - E_-(\mathbf{q}))/\hbar$; here $E_+(\mathbf{q})$ and $E_-(\mathbf{q})$ are the adiabatic potentials—the position-dependent eigenvalues of the diabatic potential matrix. The density matrix elements $\rho_{mn}(\Gamma, t)$ are now phase space functions, and we have written the coherence $\rho_{+-} = \alpha + i\beta$ in terms of its real and imaginary parts.

The phase space generalized densities in the adiabatic representation are again written in terms of an ensemble of N trajectories as:

$$\rho_{++}(\Gamma, t) = \frac{1}{N}\sum_{j=1}^{N} \sigma_j(t) g(\Gamma - \Gamma_j(t)) \quad (43)$$

$$\rho_{--}(\Gamma, t) = \frac{1}{N}\sum_{j=1}^{N} \left(1 - \sigma_j(t)\right) g(\Gamma - \Gamma_j(t)). \quad (44)$$

$$\alpha(\Gamma, t) = \frac{1}{N}\sum_{j=1}^{N} \alpha_j(t) g(\Gamma - \Gamma_j(t)) \quad (45)$$

$$\beta(\Gamma, t) = \frac{1}{N}\sum_{j=1}^{N} \beta_j(t) g(\Gamma - \Gamma_j(t)). \quad (46)$$

A similar analysis to the one performed above for the diabatic case then yields the CSH equations of motion for the quantum state parameters and phase space trajectories.

The stochastic parameters $\{\sigma_j\}$ $(j = 1, 2, \ldots, N)$ are updated as follows. For the jth trajectory at phase space point $\Gamma_j = (\mathbf{q}_j(t), \mathbf{p}_j(t))$ currently occupying state $|+\rangle$, the probability of hopping to state $|-\rangle$ at time t during a time interval Δt is given by

$$P_{hop}^{CSH} = \left| \frac{2}{\langle \rho_{++} \rangle} \frac{\mathbf{d}(\mathbf{q}_j) \cdot \mathbf{p}_j}{m} \langle \alpha \rangle_j \Delta t \right| \quad (47)$$

with an analogous expression for hops from $|-\rangle \rightarrow |+\rangle$. The equations of motion for the coherence parameters yield the differential equations

$$\dot{\alpha}_j = \omega(\Gamma_j)\beta_j + \frac{\mathbf{d}(\mathbf{q}_j) \cdot \mathbf{p}_j}{m}(2\sigma_j - 1) \quad (48)$$

$$\dot{\beta}_j = -\omega(\Gamma_j)\alpha_j(t). \quad (49)$$

The trajectory equations of motion for $\mathbf{q}_j(t)$ and $\mathbf{p}_j(t)$ can be derived from the equation of motion for the total nuclear density $\rho = \rho_{++} + \rho_{--}$ using the same procedure employed above in the diabatic case. The result is

$$\dot{\mathbf{q}}_j = \frac{\mathbf{p}_j}{m} - 2\hbar\beta_j \frac{\mathbf{d}(\mathbf{q}_j)}{m} \quad (50)$$

$$\dot{\mathbf{p}}_j = -\nabla U_j(\mathbf{q}_j) + \frac{2\hbar}{m}\beta_j \left(\mathbf{p}_j \cdot \nabla\right) \mathbf{d}(\mathbf{q}_j) \quad (51)$$

for $j = 1, 2, \cdots, N$. The quantum forces acting on the classical trajectories in the adiabatic representation are in the form of Hamilton's equations in the presence of a vector potential $\mathbf{A}(\mathbf{q}, \beta(t))$:

$$H(\Gamma, \sigma, \beta) = \frac{(\mathbf{p} - \mathbf{A}(\mathbf{q}, \beta(t)))^2}{2m} + U_\sigma(\mathbf{q}), \quad (52)$$

where $\mathbf{A}(\mathbf{q}, \beta(t)) = 2\hbar\beta(t)\mathbf{d}(\mathbf{q})$ (neglecting terms of order $\hbar^2$). This vector potential depends on the quantum subsystem dynamics through the appearance of the imaginary part of the coherence, $\beta_j(t)$. Interesting geometric phase effects resulting from these nonclassical forces may result in systems with two or more dimensions in the presence of, e.g., conical intersections[39–43]. This will be explored in future work.

These equations of motion are closely related to those appearing in the Miller-Meyer treatment of coupled electronic-nuclear dynamics[44–46]. In Ref.[46] Cotton *et al.* introduce a non-Hamiltonian "kinematic momentum", given in our notation by $\mathbf{p}_{kin,j} = \mathbf{p}_j - 2\hbar\beta_j\mathbf{d}(\mathbf{q}_j)$, and show that its use simplifies numerical calculations by avoiding the appearance of $\nabla\mathbf{d}$. This approach is applied in our numerical application of the present method.

The CSH method is based on a systematic derivation of the equations of motion for a trajectory ensemble representation of the nonadiabatic dynamics from the underlying quantum Liouville equation in the semiclassical limit. CSH eliminates the *ad hoc* instantaneous momentum rescaling and strict energy conservation of FSSH by incorporating continuous state-dependent quantum forces into the trajectory equations of motion. In addition, the inclusion of quantum coherence and decoherence emerges naturally in the CSH formalism through the collective and interdependent nature of the trajectories across the ensemble in determining hopping probabilities.

The numerical implementation of the method can be quite accurate for model systems[12]. However, the interdependent nature of the trajectories greatly increases the numerical cost of the method in direct implementations. For multidimensional systems, the CSH method quickly becomes prohibitively expensive with increasing size. Further, the complexity of the method can lead to errors if conditions and parameters such as the Gaussian smoothing width are not chosen carefully. The main value of CSH is not as a practical method *per se*, but as a theoretical framework for introducing further approximations in a well-controlled manner

In Ref.[13] we described a new surface hopping method, Quantum Trajectory Surface Hopping (QTSH), an approximate approach based on an *independent trajectory* limit of CSH. The QTSH stochastic hopping algorithm is identical to that of FSSH, but the *ad hoc* impulsive momentum jumps of FSSH are abandoned and replaced by the continuous quantum forces that emerge from the CSH formalism. This involves replacing the ensemble-level quantities appearing in the CSH formalism by proxy quantities, as in FSSH. in our notation, the connection between the ensemble level quantities and the density matrix probabilities a_{nn} is

$$\langle \rho_{11} \rangle_j = \frac{1}{N} \sum_{k=1}^{N} \sigma_j g(\Gamma_j - \Gamma_k) \simeq \langle \sigma \rangle_j \langle \rho \rangle_j \equiv a_{11,j} \langle \rho \rangle_j \quad (53)$$

with a similar expression relating $\rho_{22,j}$ with $a_{22,j}$, and

$$\langle \beta \rangle_j \simeq \frac{1}{N} \sum_{k=1}^{N} \beta_j g(\Gamma_j - \Gamma_k) \simeq \beta_j \langle \rho \rangle_j. \quad (54)$$

Here, $\langle \rho \rangle_j$ is the local value of the total nuclear density $\rho = \rho_{11} + \rho_{22}$ at point Γ_j. The local average value of the stochastic binary numbers representing state occupation is equated with the continuous proxy density matrix probability: $\langle \sigma \rangle_j \simeq a_{11,j}$. For the second expression, we make the simplifying assumption that the system is *fully coherent*, in the sense that the parameters β_k are slowly varying in the vicinity of Γ_j. With these approximations, we arrive at the QTSH hopping probability expression

$$P_{hop}^{QTSH}(t) = \left| \frac{1}{a_{11,j}} \frac{2V(\Gamma_j)}{\hbar} \beta_j \Delta t \right|, \quad (55)$$

which is identical to the corresponding FSSH result, Eq. (9). The consistency assumption of FSSH further assumes that the $a_{kl}(t)$ parameters can be computed by solving the auxiliary quantum equations of motion for each trajectory, Eq. (6).

A similar line of reasoning gives the QTSH hopping probability in the adiabatic representation:

$$P_{hop}^{QTSH} = \left| \frac{2}{a_{++,j}} \frac{\mathbf{d}(\mathbf{q}_j) \cdot \mathbf{p}_j}{m} \alpha_j \Delta t \right|. \quad (56)$$

The numerical implementation of the QTSH method uses the following procedure (given here for the adiabatic representation): The continuous equations, Eq. (6), for the quantum subsystem of each trajectory is integrated to determine the smoothly varying quantities $a_{++,j}$, $a_{--,j}$, α_j, and β_j. In addition, the stochastic variable σ_j is propagated using the probabilistic algorithm

in Eq. (56). The classical variables are propagated under the influence of the instantaneous Hamiltonian $H_j = \sigma_j H_{++} + (1 - \sigma_j)H_{--}$ augmented by the CSH nonclassical terms derived above, Eqs. (50) and (51). The classical forces in the equations of motion change discontinuously at the points of transition while the non-classical forces are continuous there. The resulting phase space path $(\mathbf{q}_j(t), \mathbf{p}_j(t))$ is *continuous*, unlike in the FSSH method, as we *do not rescale the momentum* to impose energy conservation.

The FSSH method for surface hopping imposes strict conservation of the classical energy of each independent trajectory: $H_j(\Gamma_j(t), t) = E_j$, where in our notation $H_j(\Gamma, t) = \sigma_j(t)H_{++}(\Gamma) + (1 - \sigma_j(t))H_{--}(\Gamma)$ and E_j is the initial classical energy. This is accomplished by the *ad hoc* rescaling of the individual trajectory momentum at the time of each hop, which imposes energy conservation on each trajectory *by hand*.

Quantum mechanics of course requires energy conservation as well, but at the state level. Further, the *full* Hamiltonian $\hat{H}$ and density matrix $\hat{\rho}$ are involved, not just the diagonal elements. The total conserved energy of the quantum system is the operator trace $E = \text{Tr}(\hat{H}\hat{\rho})$ and its quantum-classical limit is given by the corresponding classical trace

$$E(t) = \text{Tr}H\rho = \int \mathbf{H}(\Gamma)\rho(\Gamma, t)d\Gamma, \tag{57}$$

where the integral is over the $2f$-dimensional phase space. Here, both $\mathbf{H}(\Gamma)$ and $\rho(\Gamma, t)$ are 2×2 matrices of the corresponding classical-limit phase space functions. Writing this out in terms of the matrix elements in the diabatic representation gives

$$E(t) = \text{Tr}(H_{11}\rho_{11}) + \text{Tr}(H_{22}\rho_{22}) + 2\text{Tr}(V\alpha). \tag{58}$$

The total energy consists of three terms:

$$E = E_1 + E_2 + E_{coh}. \tag{59}$$

In terms of the trajectory representation, this becomes

$$E = \frac{1}{N}\sum_{j=1}^{N} \sigma_j H_{11}(\Gamma_j) + (1 - \sigma_j)H_{22}(\Gamma_j) + 2V(\Gamma_j)\alpha_j, \tag{60}$$

The diagonal energy is the sum $E_{diag} = E_1 + E_2$. It should be noted that the total energy E is *not* equal to E_{diag}. This diagonal energy is the quantity that FSSH rigorously conserves at the individual trajectory level by momentum rescaling. When coherence $\alpha_j \neq 0$ and the coupling $V(\Gamma_j)$ is present, a third *coherence energy* term E_{coh} is required to balance the energy budget[14].

The QTSH method conserves this energy on average at the level of the consistency of the surface hopping approach:

$$\dot{E}(t) = \frac{1}{N}\sum_{j=1}^{N} \dot{E}_j(t) = 0, \tag{61}$$

where

$$\dot{E}_j(t) = \dot{\mathbf{p}}_j \cdot \frac{\mathbf{p}_j}{m} + \dot{\sigma}_j \left[U_1(\mathbf{q}_j) - U_2(\mathbf{q}_j)\right]$$
$$+ \dot{\mathbf{q}}_j \cdot \left[\sigma_j \nabla U_1(\mathbf{q}_j) + (1 - \sigma_j)\nabla U_2(\mathbf{q}_j) + 2\nabla V(\mathbf{q}_j)\alpha_j\right] + 2V(\mathbf{q}_j)\dot{\alpha}_j. \tag{62}$$

From the equations of motion for the density matrix elements we have

$$\dot{\sigma}_j \simeq \dot{a}_{11,j} = -\frac{2V(\mathbf{q}_j)}{\hbar}\beta_j \tag{63}$$

$$\dot{\alpha}_j = \omega(\mathbf{q}_j)\beta_j = \frac{1}{\hbar}\left[U_1(\mathbf{q}_j) - U_2(\mathbf{q}_j)\right]\beta_j, \tag{64}$$

where we have used $\omega = (H_{11} - H_{22})/\hbar$ and have indicated that the first equation holds *on average*.

For the phase space variables $(\mathbf{q}_j, \mathbf{p}_j)$ we have the quantum trajectory equation of motion

$$\dot{\mathbf{q}}_j = \frac{\mathbf{p}_j}{m} \tag{65}$$

$$\dot{\mathbf{p}}_j = -\left[\sigma_j \nabla U_1(\mathbf{q}_j) + (1 - \sigma_j)\nabla U_2(\mathbf{q}_j)\right] - 2\nabla V(\mathbf{q}_j)\alpha_j. \tag{66}$$

By eliminating $\dot{\mathbf{q}}_j$, $\dot{\mathbf{p}}_j$, $\dot{\sigma}_j$ and $\dot{\alpha}_j$ from the equation for $\dot{E}_j$, we can show the time derivative of each term vanishes on average, $\dot{E}_j \simeq 0$, so that

$$\dot{E}(t) = 0. \tag{67}$$

It should be noted that this energy conservation, which holds rigorously if $\sigma_j(t)$ evolves continuously, is *not* strictly obeyed at the individual trajectory level when a stochastic algorithm is employed to propagate σ_j. A sudden "hop" of $\sigma_j(t) = 0$ to $\sigma_j(t) = 1$, for instance, leads to an instantaneous change in the Hamiltonian $H_j = \sigma_j H_{11} + (1 - \sigma_j)H_{22}$ from H_{11} to H_{22}. However, on average, σ_j obeys the smooth differential equation, and so averaged over the ensemble the energy conservation of the *state* re-emerges. The assumptions required for this *quantum* energy conservation are equivalent to the consistency assumption underlying the surface hopping method itself.

The same approach can be followed to show the average energy conservation in the adiabatic representation[13,14].

3 Numerical Simulations and Discussion

We now examine the peformance of the FSSH and QTSH methods in detail for a number of very simple systems and compare with exact quantum wavepacket calculations. We look at the time-dependent populations of the coupled electronic states and perform an audit of the energy budget for the QTSH and quantum simulations. In addition, we visualize the evolving trajectory ensembles in phase space and compare with the Wigner transforms of the exact quantum wavepackets.

The coupled state quantum dynamics calculations are performed in the diabatic representation using the Fourier transform-based method of Kosloff[47], and transformed to the adiabatic representation when appropriate. The Wigner transforms of the resulting wavepackets are computed numerically as well. For a wavepacket $\psi_n(q, t)$ on the (diabatic or adiabatic) state n at time t, the corresponding Wigner transform representing the phase space density $\rho_{nn}(q, p, t)$ is given by

$$\rho_{nn}(q, p, t) = \frac{1}{\pi\hbar}\int_{-\infty}^{\infty} \psi_n(q - y, t)\psi^*(q + y, t)e^{2ipy/\hbar}dy. \tag{68}$$

We treat a number of two state coupled systems, whose Hamil-

tonians can be written in the diabatic representation as:

$$\hat{H} = \begin{pmatrix} \hat{T} + U_1(q) & V(q) \\ V(q) & \hat{T} + U_2(q) \end{pmatrix}, \qquad (69)$$

where $\hat{T} = \frac{\hat{p}^2}{2m}$ is the nuclear kinetic energy operator, $U_1(q)$ and $U_2(q)$ are state 1 and 2 diabatic potential, respectively, and $V(q)$ is the off-diagonal diabatic potential coupling. For all cases we take the mass to be $m = 2000$, the same as in Tully's original paper[1]. (We use atomic units throughout.) The initial wavepacket is taken to be a minimum uncertainty Gaussian localized at an initial position q_o with an initial mean momentum $p_o = \hbar k$. The position and momentum widths are $\Delta q = 1.0$ and $\Delta p = 0.5$, respectively. For the QTSH and FSSH simulations ensembles of $N = 10000$ are employed. These are sampled randomly from the initial Gaussian Wigner function in phase space. When visualizing the ensembles, typically every other point is shown to avoid congestion on the figure. Each calculation shown is easily done interactively in a few minutes or less on a laptop.

3.1 Two state constant coupling model

We start with a very simple model of nuclear wavepacket dynamics on two constant parallel diabatic states with constant coupling. For this system, the potential matrix elements are all constant, with values $U_1 = 0$, $U_2 = 0.01$, and $V = 0.01$.

In this simple system, the exact nuclear wavepacket and electronic population dynamics decouple, leading to trivial behavior with a free particle nuclear wavepacket evolving and spreading while the electronic state populations undergoes Rabi oscillations[22]. The system nonetheless provides a nontrivial test for the surface hopping methods and illustrates some important features of each.

In Fig. 1 we show the population dynamics of the two state constant coupling model for a wavepacket starting initially on the lower state 1 with mean position $q_o = -6$ and mean momentum $p_o = \hbar k = 10$. The results of QTSH (blue dashed lines) and FSSH
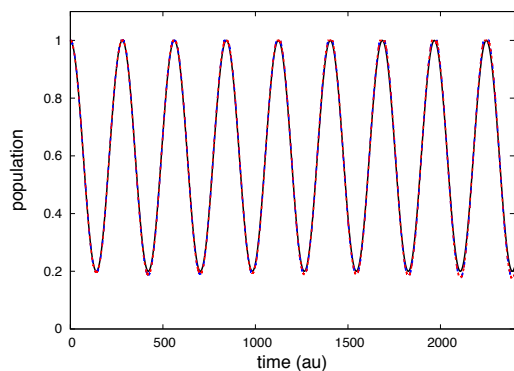
Fig. 1 Lower state 1 population *vs.* time for the two state constant coupling model. The system starts initially in the lower state 1 with momentum $\hbar k = 10$. QTSH (blue dashed) and FSSH (red dashed) results are compared with exact quantum calculations (black solid).

(red dashed lines) are presented, along with the exact quantum results (black solid lines). All the curves are essentially identical, and exhibit the periodic Rabi oscillation of probability out of and into the initially populated state 1. The quantum electronic component of the dynamics is captured essentially exactly by both surface hopping methods.

In Fig. 2 we present an accounting of the energy budget for the system (see Eqs. (59) and (60)). Here, we compare the QTSH
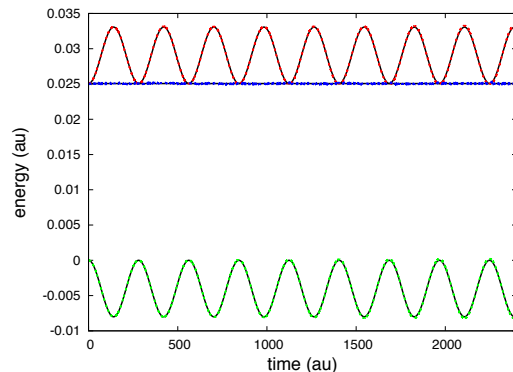

Fig. 2 The energy budget for the QTSH simulation shown in Fig. 1. The diagonal (red), coherence (green), and total (blue) energies for the trajectory ensemble are compared with the exact quantum counterparts (black).

results with corresponding exact quantum results. We show the diagonal E_{diag} (red) and coherence E_{coh} (green) contributions, as well as the total $E = E_{diag} + E_{coh}$. These are compared with the corresponding partitioning of the exact quantum energy (black). The agreement here is nearly quantitative. The Figure clearly shows that it is the total energy $\text{Tr}\hat{H}\hat{\rho}$ that is conserved by the evolution. The classical diagonal energy, consisting of the kinetic plus diagonal potential energies, is *not* a conserved quantity.

In Figs. 3–5 we investigate in more detail the nature of the dynamics and its relation to the energy budget from a phase space perspective. In Fig. 3 we show snapshots of the evolving state 1 a)-d) and state 2 e)-h) wavepackets in the Wigner representation. The times of each snapshot are indicated in the caption. Fig. 3 a) shows the initial minimum uncertainty wavepacket in phase space on state 1. The state 2 population is zero initially, and so the Wigner function vanishes in Fig. 3 e). Subsequent frames shows the expected motion: free particle translation and phase space shearing, accompanied by Rabi oscillation of the population between states. In particular, the wavepacket has a conserved mean momentum and kinetic energy throughout its evolution.

In Fig. 4 we reproduce the Wigner function snapshots for this system, but now with the evolving QTSH ensemble overlaid for comparison (black dots). The agreement between the QTSH and quantum states of this system are nearly quantitative. For this system, the coupling V is a constant, and so the quantum force appearing in Eq. (29) vanishes. The dynamics of the ensemble between hops is thus simply free *classical* motion. When a hop does occur, QTSH does not implement a classical energy conserv-
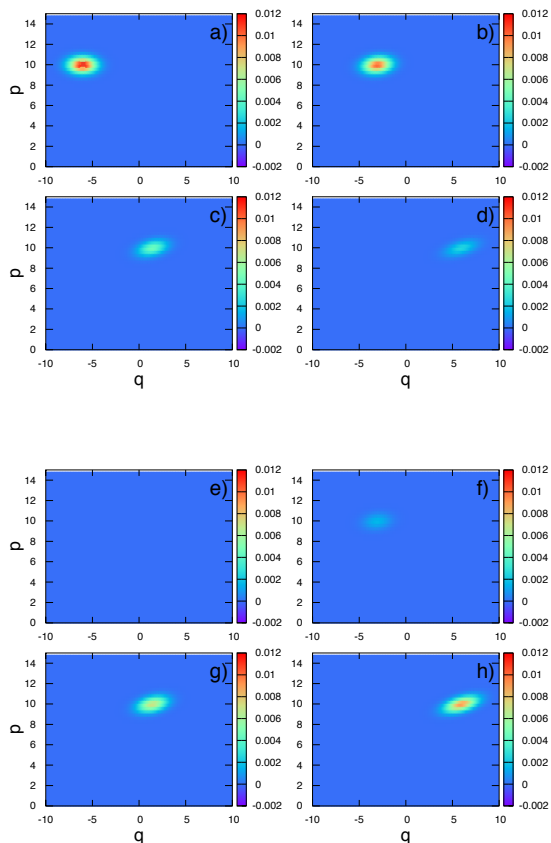
Fig. 3 Phase space contour plots of the evolving state 1 (a-d) and state 2(e-h) Wigner functions, for the two state constant coupling model with initial state as in Fig. 1. a,e) $t = 0$. b,f) $t = 600$. c,g) $t = 1500$. d,g) $t = 2400$.
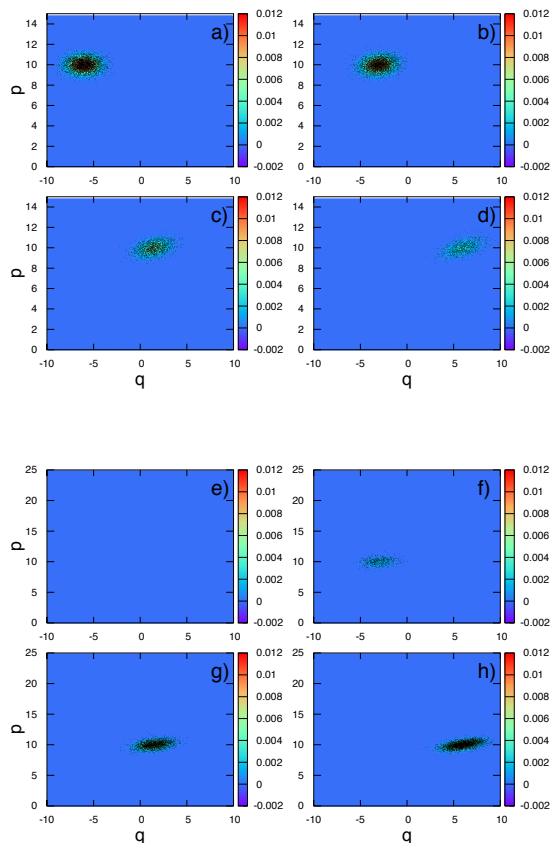

Fig. 4 Contour plots of evolving Wigner functions reproduced from Fig. 3 with corresponding QTSH ensembles overlaid (black points).

ing momentum rescaling, and so the trajectory continues with its conserved classical momentum.

In Fig. 5 we compare the exact Wigner function snapshots on state 1 and 2 with the corresponding FSSH ensembles. Clear deviations between the classical and quantum densities is observed, which can be understood by considering the effect of energy conserving momentum rescaling. Examining first the oscillating density transferred to and from the upper state 2 in Fig. 5 e)–h), we see that the classical density is displaced in both momentum and position from the exact Wigner function. This error is due to the imposition of classical energy conservation, which causes a negative momentum jump that displaces the ensemble to lower momenta and also delays its dynamical progress in configuration space. The lower state FSSH density is also shifted from the exact quantity. Here, the momentum distribution is accurate, with the error being in the coordinate q. This is the result of the slowed progress of the trajectories when on the upper surface due to the momentum rescaling of FSSH.

For the initial momentum $\hbar k = 10$ example shown above, most of the trajectories in the surface hopping ensembles have sufficient kinetic energy to undergo a FSSH-allowed classical energy conserving hop to the upper surface. This leads to the agreement of both QTSH and FSSH with the exact quantum population

transfer, shown in Fig. 1.

In Fig. 6 we consider a lower energy state, with $\hbar k = 6$. The time dependent population of the initially populated lower state from the QTSH and FSSH simulations are compared with the exact quantum results. The electronic and nuclear dynamics for this system decouple, and so the behavior should be identical to that in Fig. 1. The QTSH population dynamics are still in excellent agreement with the quantum behavior, while FSSH strongly underestimates the extent of transfer. For $\hbar k = 6$, a majority of the trajectories are classically forbidden to undergo a hop under the FSSH algorithm. Nonetheless, the quantum nature of the process allows transfer to occur just as extensively as for the $\hbar k = 10$ case.

This system can be treated in the adiabatic representation as well. The constant potential matrix is diagonalized by a transformation that is coordinate independent, leading to zero nonadiabatic coupling and the (trivial) dynamics of free particle motion on the initially populated adiabatic state.

3.2 Two state Gaussian coupling model

We consider next a system that is still very simple but where electronic-nuclear coupling is present. In particular, we take the same two state constant potential system treated above, with $U_1 = 0$ and $U_2 = 0.01$, but add coordinate dependence to the off diagonal diabatic potential coupling: $V(q) = c \exp(-dq^2)$, where
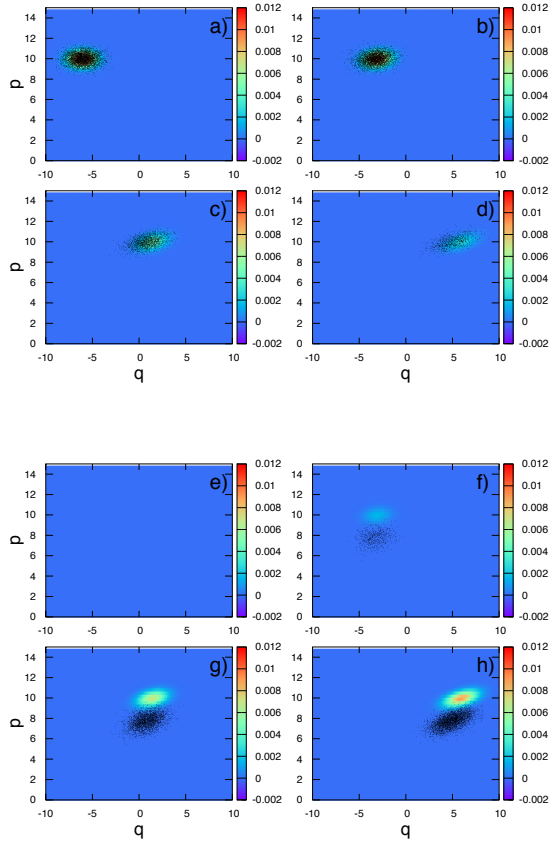
Fig. 5 Contour plots of evolving Wigner functions reproduced from Fig. 3 with corresponding FSSH ensembles overlaid (black points).
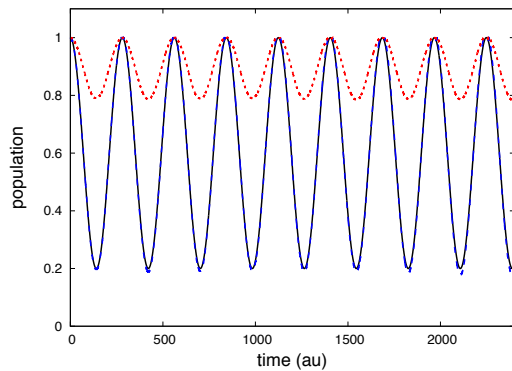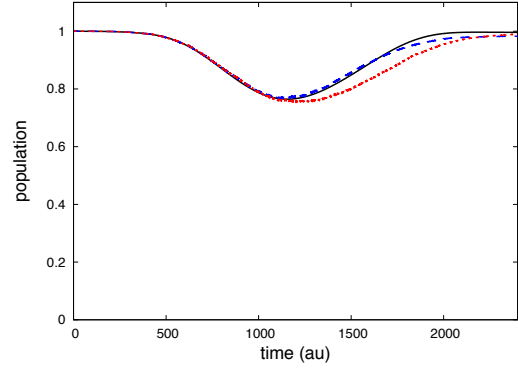

Fig. 6 Lower state population *vs.* time for the two state constant coupling model. The system starts initially on the lower state 1 with momentum $\hbar k = 6$. QTSH (blue dashed) and FSSH (red dashed) results are compared with exact quantum calculations (black solid.

$c = 0.01$ and $d = 0.25$,

In Fig. 7 we show the lower state 1 population for the two state Gaussian coupling model, with initial mean position $q_o = -6$ and initial mean momentum $\hbar k = 10$. The QTSH (blue dashed) and FSSH (red dashed) results are compared with exact quantum

Fig. 7 Lower state population *vs.* time for the two state Gaussian coupling model. System starts initially in the lower state 1 with momentum $\hbar k = 10$. QTSH (blue dashed) and FSSH (red dashed) results are compared with exact quantum calculations (black solid).

calculations (black solid). Good qualitative agreement is seen between the surface hopping and exact quantum results, with QTSH being in better quantitative agreement. The coupling between the diabatic states is localized around $q = 0$, leading to population transfer only in that region.

In Fig. 8 we show the energy audit of this system with initial momentum $\hbar k = 10$. The classical diagonal (red), coherence

Fig. 8 The energy budget for the QTSH simulation of the two state Gaussian coupling model shown in Fig. 7. The diagonal (red), coherence (green), and total (blue) energies for the trajectory ensemble are compared with the exact quantum counterparts (black).
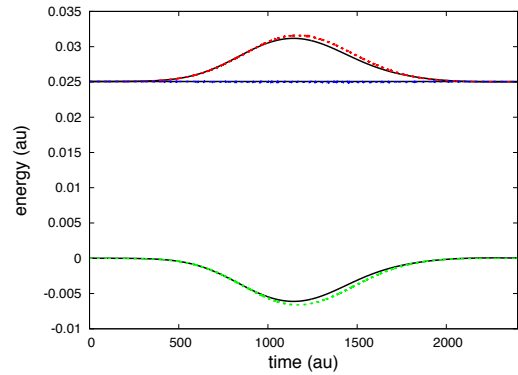
(green), and total (blue) energies for the trajectory ensemble are compared with the exact quantum counterparts (black). The Figure highlights the strong positive nonconservation of the classical energy during the transition as probability is transferred to the upper surface *without* a decrease in momentum, and the correspondingly large negative coherence energy, which add to a strictly conserved total $E = \mathrm{Tr}\hat{H}\hat{\rho}$. The QTSH method faithfully captures these effects.

Figs. 9–11 show the comparisons of the evolving QTSH and FSSH trajectory ensembles with the exact Wigner functions for

wavepackets on state 1 and 2 for the two state Gaussian coupling model, in the same manner as Figs. 3–5 above. Again, the QTSH
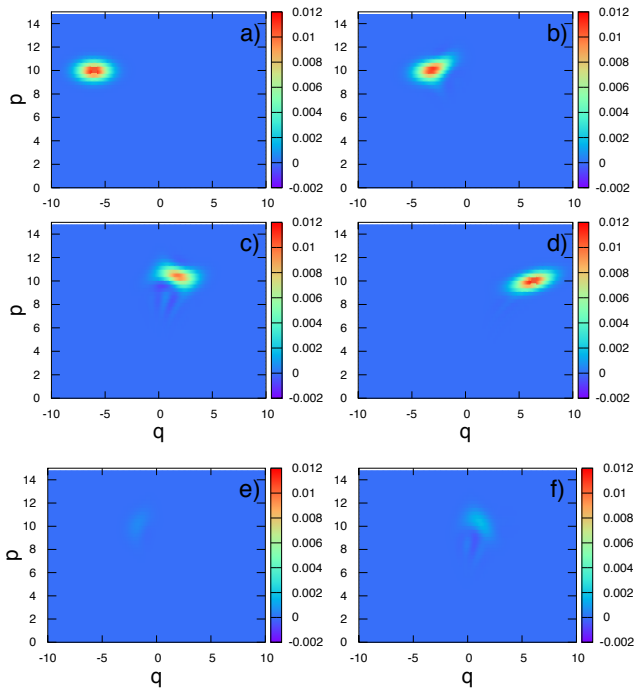

Fig. 9 Phase space contour plots of the evolving state 1 (a-d) and state 2 (e,f) Wigner functions, for the two state Gaussian coupling model with initial state as in Fig. 7. a) $t = 0$. b,e) $t = 600$. c,f) $t = 1500$. g) $t = 2400$.
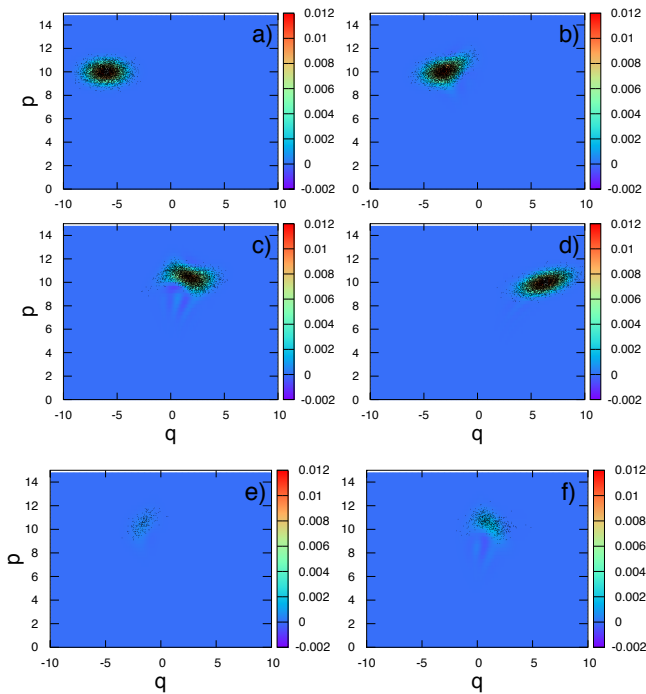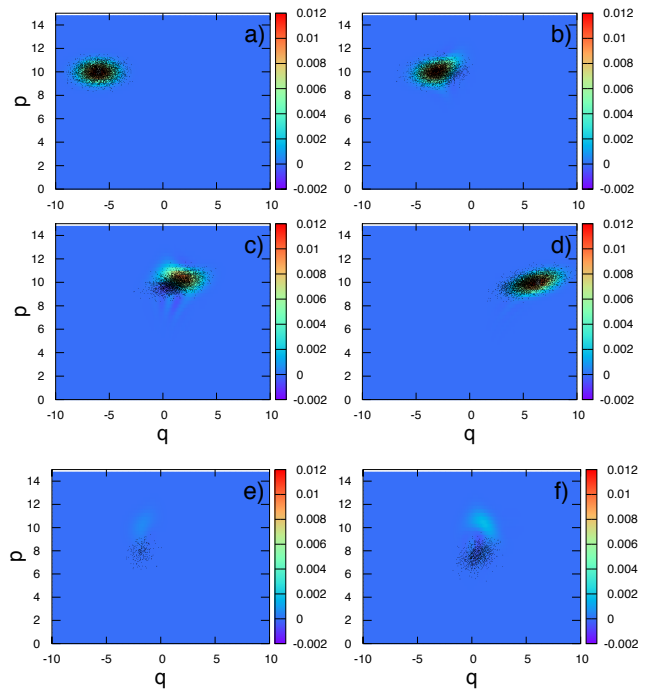

Fig. 10 Contour plots of evolving Wigner functions reproduced from Fig. 9 with corresponding QTSH ensembles overlaid (black points).

method faithfully captures the nonclassical nature of the quantum transfer between the states, while FSSH shows a distinct dis-

Fig. 11 Contour plots of evolving Wigner functions reproduced from Fig. 9 with corresponding FSSH ensembles overlaid (black points).

placement of the ensemble from the Wigner function due to the incorporation of momentum jumps (see, in particular Fig. 11 f)).

In Fig. 12 we show the time-dependent population of lower diabatic state 1 for the two state Gaussian coupling model with a less energetic initial momentum of $\hbar k = 6$. The QTSH (blue) and
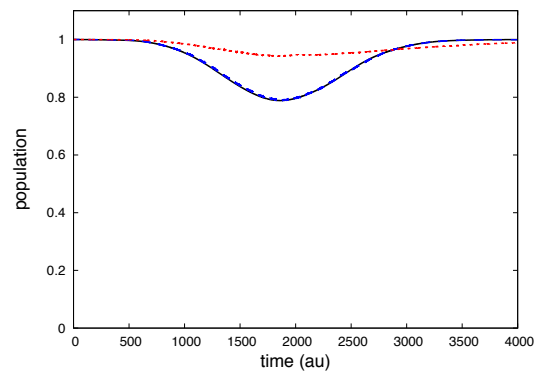

Fig. 12 Lower diabatic state 1 population *vs.* time for the two state Gaussian coupling model. The system starts initially on the lower state 1 with momentum $\hbar k = 6$. QTSH (blue dashed) and FSSH (red dashed) results are compared with exact quantum calculations (black solid.

FSSH (red) results are compared with the exact quantum results (black). QTSH again captures the transient population transfer to and from state 2 nearly quantitatively. As in the example shown above for the constant coupling model with initial momentum $\hbar k = 6$, most of the initial trajectories are classically forbidden to transfer to the upper diabatic state, and so most FSSH hops are

frustrated. The result of this is a large error in the state population dynamics.

The previous two examples are both characterized by large nonclassical effects in the coupled electronic-nuclear dynamics. In addition, the calculations are performed in the diabatic representation rather than the more commonly-employed adiabatic representation. The QTSH formalism has the advantage of being well-defined in the diabatic and adiabatic (or any arbitrary) representation, while the FSSH momentum rescaling relies on the nonadiabatic coupling vector to define the direction of the momentum jumps in multidimensional systems.

3.3 Constant plus linear Gaussian coupling model

In the next example, we consider a model of a classically allowed energy relaxation process, and perform surface hopping calculations in the adiabatic representation. The model is a coupled constant and linear potential, with Gaussian diabatic coupling. In particular, we take $U_1 = 0$, $U_2(q) = -aq$, and $V(q) = c\exp(-dq^2)$, with $a = 0.005$, $c = 0.001$, and $d = 0.25$. The adiabatic potentials are determined by computing the coordinate dependent eigenvalues of the potential matrix, while the nonadiabatic coupling $d(q)$ is found from the coordinate dependence of the electronic adiabatic states (see Ref. [13] for more details). The relatively small diabatic coupling leads to a correspondingly strong nonadiabatic coupling.

In Fig. 13 we show population transfer in the adiabatic representation for the constant plus linear Gaussian coupling model. The system starts initially on the upper adiabatic surface with a
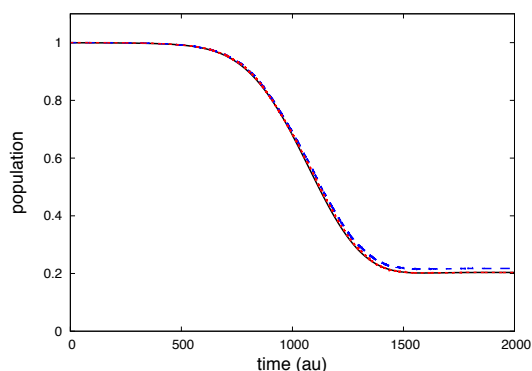

Fig. 13 Lower adiabatic state populations *vs.* time for the constant plus linear potential Gaussian coupling model. Simulations are performed in the adiabatic representation. System starts initially in the upper adiabatic state with momentum $\hbar k = 6$. QTSH (blue dashed) and FSSH (red dashed) results are compared with exact quantum calculations (black solid.

mean position of $q_o = -4, 0$ and mean momentum of $p_o = \hbar k = 5$. As the wavepacket passes through the avoided crossing around $q = 0$ approximately 80 percent of the population is transferred to the lower surface. This energy relaxation process is classically allowed, and both surface hopping methods agree well with the exact quantum results, with FSSH being in essentially quantita-

tive agreement.

The energy budget for the time evolution of the $\hbar k = 5$ initial state is shown in Fig. 14. This example shows less contribution
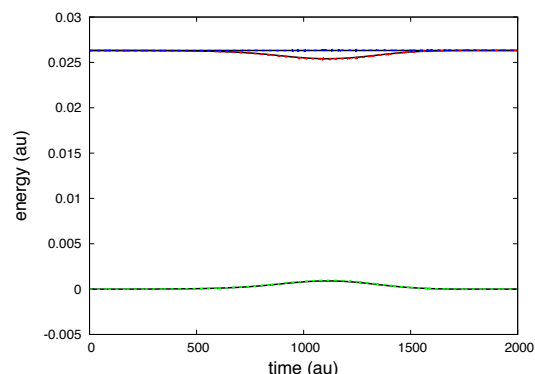

Fig. 14 The energy budget in the adiabatic representation for the QTSH simulation of the constant plus linear potential Gaussian coupling model shown in Fig. 13. The diagonal (red), coherence (green), and total (blue) energies for the trajectory ensemble are compared with the exact quantum counterparts (black).

from the coherence energy than in the previous cases, but the effect is still visible. Here, the diagonal energy exhibits a negative change during the nonadiabatic transition. This corresponds to a decrease in the potential energy with the nonadiabatic transition, and the negative sign suggests that this downward hop should *not* be compensated for by a positive momentum jump. QTSH correctly captures his aspect of the dynamics, and the total energy is conserved well without the intervention of any momentum rescaling.

In Figs. 15–17 we again give a comparison of the evolving QTSH and FSSH trajectory ensembles with the exact Wigner functions. Here, the ensembles and the exact Wigner functions are displayed in the adiabatic representation. Accurate quantum-classical correspondence between the exact wavepackets in the Wigner representation and the trajectory swarms is achieved for both the QTSH and FSSH approaches in this more classical process.

4 Conclusions

In this paper, we have presented a detailed investigation of the population transfer, energetics, and phase space dynamics of the Fewest Switches Surface Hopping (FSSH) and Quantum Trajectory Surface Hopping (QTSH) methods for simulating molecular dynamics with electronic transitions. Comparisons were made between these trajectory ensemble-based approaches and exact quantum calculations for a number of simple model problems.

Nonadiabatic dynamics of molecular systems is an important physical process that arises in many practical applications. The topic is also of fundamental interest, as it challenges theory to understand deeply the correspondence principle and the semiclassical limit of quantum mechanics. Successful practical methods result from finding an amenable cohabitation of quantum mechani-
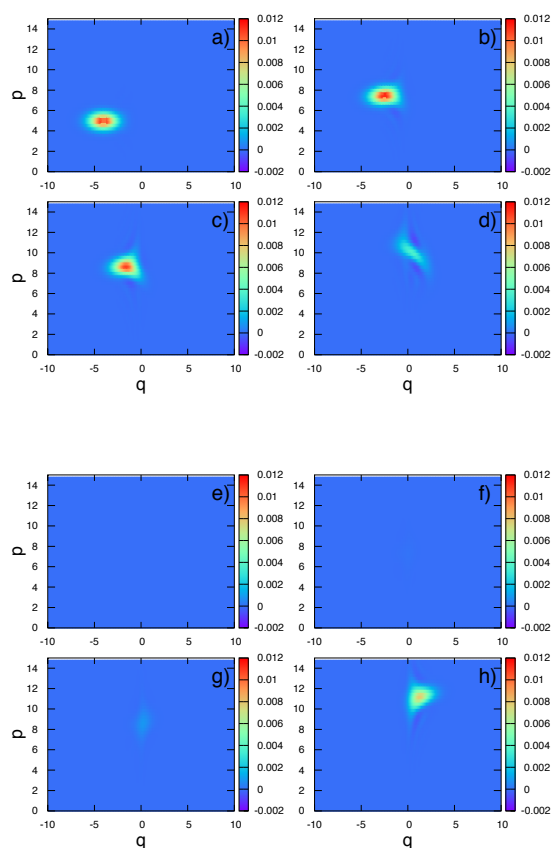
Fig. 15 Phase space contour plots of the Wigner functions of the evolving adiabatic upper (a-d) and lower (e-h) states for the constant plus linear potential Gaussiancoupling model with initial state as in Fig. 13. a,e) $t = 0$, b,f) $t = 500$, c,g) $t = 750$, and d,g) $t = 1250$.

Fig. 16 Contour plots of evolving Wigner functions reproduced from Fig. 15 with corresponding QTSH ensembles overlaid (black points).

cal and classical descriptions of nature within the same theoretical framework. The dynamics of coupled electronic-nuclear motion in molecules spans both sides of the quantum-classical border.

The two state constant and Gaussian coupling models treated above highlight clearly the role of nonclassical dynamics and energetics in coupled electronic-nuclear motion. Here, electronic coherence and off-diagonal coupling work together to play an essential role in the overall energy conservation, allowing the diagonal (classical) part of the system to effectively ignore energetic constraints while undergoing its dynamics. The highly classical framework of FSSH leads to its failure for processes in this nonclassical regime. On the other hand, the QTSH method treats energy conservation in a fundamentally different manner *via* the quantum forces coupling electronic and nuclear dynamics derived from the semiclassical limit of the quantum Liouville equation. The QTSH results for these systems are in essentially quantitative agreement with the exact quantum calculations, showing the ability of the quantum trajectory-based surface hopping approach to go beyond the classical limit to capture nonclassical effects.

For the energy relaxation of the constant plus linear Gaussian coupling model, the dynamics are more classical, exhibiting energetically allowed downward hops and a small (but nonzero)
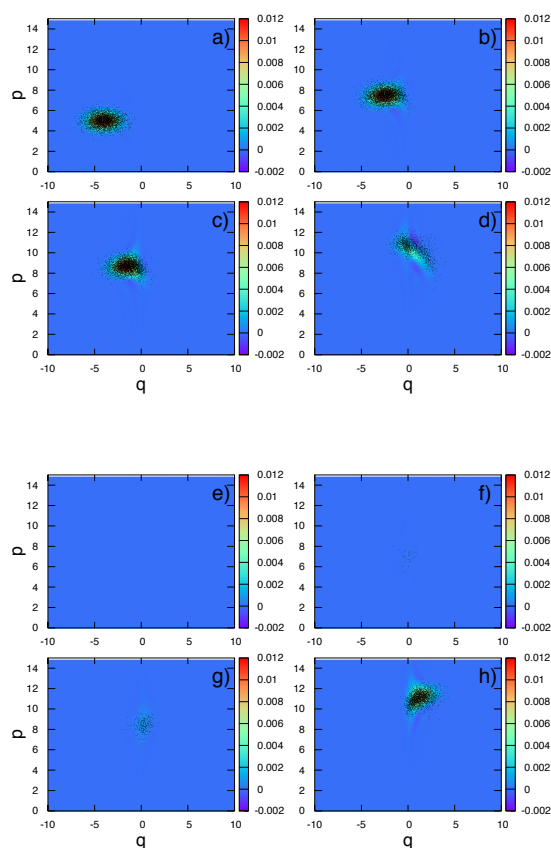
role played by the coherence contribution to the total energy. For this example, both QTSH and FSSH are in close agreement with the exact quantum results. In this more classical case, the physically motivated FSSH algorithm becomes essentially equivalent to the QTSH method. We have shown in previous work on more complicated systems that FSSH can be more accurate than QTSH in some cases [13]. For QTSH, the energetic boundary conditions that are contained automatically in FSSH must emerge through an interplay between the quantum forces and the coherence of the ensemble. The QTSH method is an approximate independent trajectory limit of CSH, and so suffers from the same problems of overcoherence that FSSH has. Apparently, the energy constraints resulting from the frustrated hops that FSSH incorporates "by hand" help to counteract the shortcomings in the treatment of the collective nature of coherence and energetics suffered by independent trajectory surface hopping methods in general.

Both QTSH and FSSH have their respective realms of preference in practical applications, the former being better for processes where nonclassical effect dominate and the latter where the complexity of the system breaks down approximations in independent ensemble methods in a way that can be repaired by strict classical energy accounting. From a fundamental conceptual perspective, these differences inspire further work on this fascinating problem at the quantum-classical border.
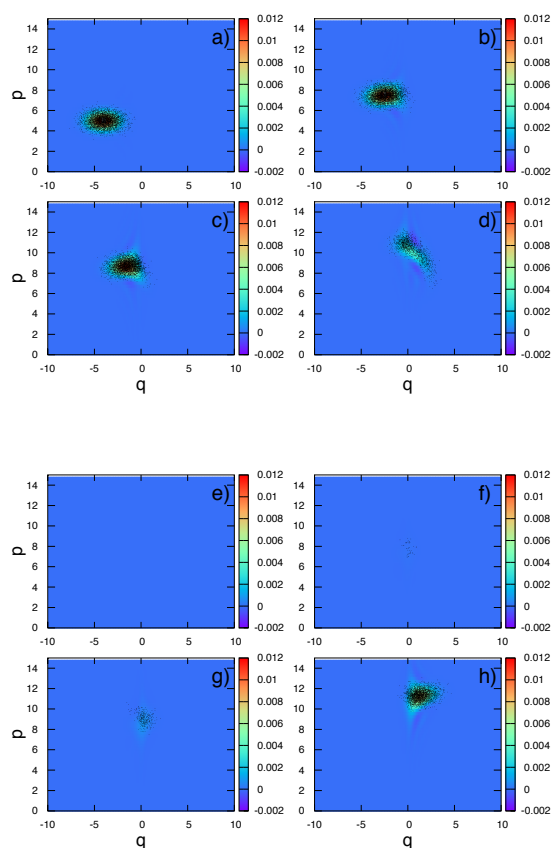
Fig. 17 Contour plots of evolving Wigner functions reproduced from Fig. 15 with corresponding FSSH ensembles overlaid (black points).

Conflicts of interest

There are no conflicts to declare.

Acknowledgements

Notes and references

1   J. C. Tully, *J. Chem. Phys.*, 1990, **93**, 1061.

2   J. C. Tully, *J. Chem. Phys.*, 2012, **137**, 22A301.

3   J. E. Subotnik and N. Shenvi, *J. Chem. Phys.*, 2011, **134**, 024105.

4   H. M. Jaeger, S. Fischer and O. V. Prezhdo, *J. Chem. Phys.*, 2012, **137**, 22A545.

5   J. E. Subotnik, W. Ouyang and B. R. Landry, *J. Chem. Phys.*, 2013, **139**, 214107.

6   B. F. E. Curchod and I. Tavernelli, *J. Chem. Phys.*, 2013, **138**, 184112.

7   A. K. Belyaev, C. Lasser and G. Trigila, *J. Chem. Phys.*, 2014, **140**, 224108.

8   H.-T. Chen and D. R. Reichman, *J. Chem. Phys.*, 2016, **144**, 094104–10.

9   L. Wang, A. Akimov and O. V. Prezhdo, *J. Phys. Chem. Lett.*, 2016, **7**, 2100–2112.

10 J. E. Subotnik, A. Jain, B. Landry, A. Petit, W. Ouyang and N. Bellonzi, *Ann. Rev. Phys. Chem.*, 2016, **67**, 387–417.

11 R. Crespo-Otero and M. Barbatti, *Chem. Rev.*, 2018, **118**, 7026–7068.

12 C. C. Martens, *J. Phys. Chem. Lett.*, 2016, 2610–2615.

13 C. C. Martens, *J. Phys. Chem. A*, 2019, **123**, 1110–1128.

14 C. C. Martens, *Chem. Phys.*, 2016, **481**, 60–68.

15 C. C. Martens and J. Y. Fang, *J. Chem. Phys.*, 1997, **106**, 4918–4930.

16 A. Donoso and C. C. Martens, *J. Phys. Chem. A*, 1998, **102**, 4291–4300.

17 A. Donoso and C. C. Martens, *J. Chem. Phys.*, 2000, **112**, 3980–3989.

18 A. Donoso, D. Kohen and C. C. Martens, *J. Chem. Phys.*, 2000, **112**, 7345–7354.

19 A. Donoso and C. C. Martens, *Int. J. Quantum Chem.*, 2002, **87**, 1348–1360.

20 R. Kapral and G. Ciccotti, *J. Chem. Phys.*, 1999, **110**, 8919.

21 S. Nielsen, R. Kapral and G. Ciccotti, *J. Chem. Phys.*, 2000, **112**, 6543.

22 C. Cohen-Tannoudji, B. Diu and F. Laloe, *Quantum Mechanics*, Wiley, New York, 1977.

23 D. A. McQuarrie, *Statistical Mechanics*, HarperCollins, New York, 1976.

24 K. Takahashi, *Prog. Theor. Phys. Suppl.*, 1989, **98**, 109–156.

25 S. Mukamel, *Principles of Nonlinear Optical Spectroscopy*, Oxford University Press, Oxford, 1995.

26 J. M. Riga and C. C. Martens, *J. Chem. Phys.*, 2004, **120**, 6863–6873.

27 J. M. Riga, E. Fredj and C. C. Martens, *J. Chem. Phys.*, 2005, **122**, 174107.

28 J. M. Riga and C. C. Martens, *Chem. Phys.*, 2006, **322**, 108–117.

29 J. Riga, E. Fredj and C. Martens, *J. Chem. Phys.*, 2006, **124**, 064506.

30 P. A. Hogan, E. Fredj and C. C. Martens, *Chem. Phys. Lett.*, 2011, **510**, 208–211.

31 E. Roman and C. C. Martens, *J. Chem. Phys.*, 2004, **121**, 11572.

32 C. C. Martens, *J. Chem. Phys.*, 2015, **143**, 141101.

33 A. Donoso and C. C. Martens, *Phys. Rev. Lett.*, 2001, **87**, 223202.

34 A. Donoso and C. C. Martens, *J. Chem. Phys.*, 2002, **116**, 10598.

35 A. Donoso, Y. Zheng and C. C. Martens, *J. Chem. Phys.*, 2003, **119**, 5010.

36 P. Hogan, A. V. Wart, A. Donoso and C. C. Martens, *Chem. Phys.*, 2010, **370**, 20.

37 K. Ando, *Chem. Phys. Lett*, 2002, **360**, 240–242.

38 K. Ando and M. Santer, *J. Chem. Phys.*, 2003, **118**, 10399–10406.

39 I. G. Ryabinkin, C.-Y. Hsieh, R. Kapral and A. F. Izmaylov, *J. Chem. Phys.*, 2014, **140**, 084104.

40 I. G. Ryabinkin, L. Joubert-Doriol and A. F. Izmaylov, *J. Chem. Phys.*, 2014, **140**, 214116–12.

41 I. G. Ryabinkin, L. Joubert-Doriol and A. F. Izmaylov, *Acc. Chem. Res.*, 2017, **50**, 1785–1793.

42 C. Xie, B. K. Kendrick, D. R. Yarkony and H. Guo, *J. Chem. Theory Comput.*, 2017, **13**, 1902–1910.

43 B. K. Kendrick, J. Hazra and N. Balakrishnan, *Nature Comms.*, 2015, **6**, 7918–7.

44 H. D. Meyer and W. H. Miller, *J. Chem. Phys.*, 1979, **70**, 3214.

45 S. J. Cotton and W. H. Miller, *J. Chem. Phys.*, 2013, **139**, 234112.

46 S. J. Cotton, R. Liang and W. H. Miller, *J. Chem. Phys.*, 2017, **147**, 064112–11.

47 R. Kosloff, *Ann. Rev. Phys. Chem.*, 1994, **45**, 145.